Published in final edited form as:
Int J Radiat Oncol Biol Phys. 2010 September 1; 78(1): 280–287. doi:10.1016/j.ijrobp.2009.11.025.

Toward a real-time in vivo dosimetry system using plastic scintillation detectors

Louis Archambault, Ph.D.[*], **Tina M. Briere, Ph.D.**[*], **Falk Pönisch**[*], **Luc Beaulieu, Ph.D.**[†], **Deborah A. Kuban, M.D.**[‡], **Andrew Lee, M.D.**[‡], and **Sam Beddar, Ph.D.**[*]

[*]Department of Radiation Physics, The University of Texas M.D. Anderson Cancer Center, Houston, TX, USA

[†]Department of Radiation Oncology, The University of Texas M.D. Anderson Cancer Center, Houston, TX, USA

[‡]Département de Radio-oncologie, Centre Hospitalier Universitaire de Québec, Québec, Québec, Canada

Abstract

Purpose—In this work, we present and validate a plastic scintillation detector (PSD) system designed for real-time multi-probe *in vivo* measurements.

Methods and Materials—The PSDs were built with a dose-sensitive volume of 0.4 mm^3. PSDs were assembled into modular detector patches, each containing 5 closely packed PSDs. Continuous dose readings were performed every 150 ms, with a gap between consecutive readings of less than 0.3 ms. We first studied the effect of electron multiplication. We then assessed system performance in acrylic and anthropomorphic pelvic phantoms.

Results—The PSDs are compatible with clinical rectal balloons and are easily inserted into the anthropomorphic phantom. With an electron multiplication average gain factor of 40, a twofold increase in the signal-to-noise ratio was observed, making near real-time dosimetry feasible. Under calibration conditions, the PSDs agreed with ion chamber measurements to 0.08%. Precision, evaluated as a function of the total dose delivered, ranged from 2.3% at 2 cGy to 0.4% at 200 cGy.

Conclusion—Real-time PSD measurements are highly accurate and precise. These PSDs can be mounted onto rectal balloons, transforming these clinical devices into *in vivo* dose detectors without modifying current clinical practice. Real-time monitoring of the dose delivered near the rectum during prostate radiation therapy should help radiation oncologists protect this sensitive normal structure.

Keywords

plastic scintillation detectors; *in vivo* dosimetry; real-time monitoring; rectal balloons

Corresponding author: Sam Beddar, Ph.D., Department of Radiation Physics, Unit-94, The University of Texas M.D. Anderson Cancer Center, 1515 Holcombe, Houston, TX 77030. (713)563-2609; beddar@mdanderson.org.

CONFLICT OF INTEREST NOTIFICATION
No conflicts of interest.

INTRODUCTION

Non-periodic and/or non-reproducible movements such as sudden anatomical changes (*e.g*. colorectal gas, stomach filling, and bowel distention), systematic displacements, or gradual anatomical changes may affect the dose coverage of the target and the protection of organs at risk near dose gradients (1). One of the best ways of quantifying these effects is through *in vivo* dosimetry (2), especially real-time dosimetry.

Interest in real-time *in vivo* dose monitoring has grown with the rise of complex and time-dependent radiation therapy modalities. Many traditional dose detectors are difficult to use *in vivo* (e.g. ion chambers) or unsuitable for real-time applications (e.g. thermoluminescent dosimeters (TLDs), conventional films), but innovative detector systems have been recently implemented. A radiochromic dose detector that monitors changes in optical density in real time has been demonstrated for *in vivo* applications (3,4). Another promising approach is based on radio-luminescence and optically stimulated luminescence (OSL) that allows continuous real-time reading of an Al_2O_3 probe as well as an integral dose reading after irradiation (5). Commercial MOSFET detector systems are also capable of performing *in vivo* measurements offline (6) and in real time (7,8). Several *in vivo* detector systems, including plastic scintillation detectors, have also been characterized for brachytherapy (9).

Plastic scintillation detectors (PSDs) are known for their unique set of strengths, including water equivalence, energy independence, dose linearity, and high spatial resolution (9–17). Water equivalence is an advantage of PSDs over inorganic detectors such as MOSFETs or OSL detectors. Compared to radiochromic detectors, PSDs show little temperature dependence in the range of clinical interest. PSDs used with photomultiplier tubes (10–12) can be read rapidly; therefore, they have been proposed for use as real-time detectors (9). However, photomultiplier-based PSDs are limited to a single or, at most, a small number of detector probes. In contrast, PSDs read with a charge-coupled device (CCD) camera can be built with a large number of detector probes (i.e. anywhere from one to several thousand) (13,14). CCD cameras also exhibit a stable response (a high voltage supply is not required and the CCD chip is usually temperature-regulated), are undamaged by ambient light and do not require any external electronics or acquisition module. One of the main drawbacks of current CCD-based PSD systems is that they require between 5 and 60+ s to acquire a precise signal, making them impractical for real-time applications.

In this paper, we present work related to the development and validation of a new CCD-based PSD system conceived for multi-probe *in vivo* measurements with an acquisition apparatus that can provide dose monitoring in real time. While the fabrication of the PSD probes was based on our earlier work (13–16), the novel acquisition apparatus is newly designed for fast applications. Improvements from our earlier (offline) PSD system include: 1) Real-time monitoring; 2) Better light collection efficiency; 3) Compact and robust setup better suited for daily clinical usage; 4) Smaller detectors (over 3 times smaller than previously reported); 5) Compatibility of the detectors with clinical rectal balloons.

The purpose of this paper is to evaluate the performance of miniature PSDs when read in real time for *in vivo* dose monitoring. We therefore focus on the precision and accuracy of dose measurements in time-varying dose delivery. Details on the use of PSDs for offline applications can be found elsewhere (9–17).

The PSD system can be used for a number of sites such as the lung, head and neck, gynecological or prostate. This work is focused on the prostate for the following reasons. We hypothesize that the real-time dose monitoring will yield a more accurate understanding

of the correlation between organ toxicity and organ dose. The relationship between dose escalation and volume of normal tissue irradiated can be more clearly established when we know the actual dose to the tissues of interest. Even if the role of rectal balloons is to reduce intrafractional motion, residual motion may subsist (20). With real-time monitoring of the dose to critical structures such as the rectum we can evaluate the clinical impact of residual motion with more information than an integral dose measured with an offline *in vivo* detector.

METHODS AND MATERIALS

PSD system design

The PSD probes were made of SCSF-3HF green-emitting, multi-clad scintillating fibers (Kuraray, Tokyo, Japan), each with 0.5 mm in diameter and 2 mm in length, yielding a dose-sensitive volume of 0.4 mm^3. The scintillating fibers were coupled to 8 m long ESKA™ plastic optical fibers (Mitsubishi, Tokyo, Japan). Because of their small size, PSDs have a high spatial resolution, which prevents dose averaging in high-dose-gradient regions. They are also less intrusive and more flexible than larger probes when used *in vivo*. Individual PSDs were assembled into “detector patches” of 5 detectors spaced 1 mm apart. These detector patches were mounted onto two types of rectal balloons (Prostate Immobilizer, Medrad, Indianola, PA), transforming these clinical devices into *in vivo* dose detectors without modifying the current clinical standard of practice (Fig. 1a–e). Although the detectors were aligned (Fig. 1–c), they could be easily positioned in more than one plane of the rectum or along any side of the rectal wall.

In each detector patch, the proximal end of each PSD was aligned in a special holder optically coupled to a Luca electron multiplying (EM) CCD camera (Andor Technology, Belfast, Ireland) for readout. The coupling is done with an objective lens (JML Optical Industries, Rochester, NY) focused on a plane containing the fibers. Objective lens coupling was chosen because it allows a large number of PSDs to be read simultaneously (13,14). However, this kind of coupling allows only about 0.5% of the scintillation light to reach the scintillator (14). This camera has light-sensitive area of 496 by 658 square pixels each with a 10μm width. Its full well capacity is 26,000 electrons with a typical readout noise of 15 electrons and a dark current of 1 electron/s/pixel at the operating temperature of −20°C. Images are digitized over 14 bits. According to the manufacturer, approximately 1.7 electrons are required to produce 1 grayscale level (GSL). Each holder can receive up to 8 PSDs, and up to 12 holders can be read simultaneously by the CCD camera. This CCD camera has a frame-transfer CCD architecture and is equipped with two identical pixel arrays: one functions as the imaging area, the other as the storage area. The imaging area, where the actual image acquisition occurs, converts incident light into electrons. After exposure, the content of all pixels is rapidly switched over to the light-shielded storage area. A second image can then be acquired in the imaging area while the image held in the storage area is read. This guarantees a time gap of 0.3 ms or less between consecutive images. The CCD camera is also capable of light amplification by electron multiplication, which is achieved by adding a special gain register to the end of the normal serial register where the pixels are read. Impact ionization in the gain register generates secondary electrons in a probabilistic fashion, producing the electron multiplication gain. We chose an acquisition time of 150 ms, corresponding to the delivery of 1.5 MU (or 1.5 cGy at the depth of maximum dose), which is of the same order as the smallest number of MUs typically delivered in a single IMRT segment.

As in our previous work (13,14), the scintillation light produced by the PSD system was decoupled from the Cerenkov light by chromatic discrimination (16–18). This technique requires measuring the raw signal (*i.e.*, the superposition of scintillation light and Cerenkov

light) produced by the PSDs with two spectral bands. Because the CCD camera is a monochrome camera, an external optical system consisting of a 45°-dichroic filter and a mirror was used to separate the emitted light into two distinct spectral bands. The light exiting each PSD was incident on the dichroic filter, which transmits wavelengths higher than 535 nm and reflects wavelengths lower than 535 nm. The transmitted light was directly incident on the CCD camera; the reflected light was incident on a mirror and re-directed toward the CCD camera (Fig. 2) producing two distinct light spots for each PSD.

Each detector patch was placed inside an acrylic phantom at d_{max} for calibration and characterization. The phantom was irradiated using a Varian 2100EX linac (Varian Medical Systems, Palo Alto, CA), with beam energy of 6 MV at a dose rate of 600 MU/min. The CCD camera was kept in the radiation vault behind a protective maze.

Images acquired with the CCD camera were processed to convert the series of light spots produced by PSDs into a dose reading. First, we acquired dark images prior to irradiation that were averaged and subtracted from the subsequent images to ensure there was no background offset.

Because stray radiation from the linac may produce artificially bright pixels on the image, images must be filtered before quantitative analysis is performed. In a previous study, we characterized radiation-induced transient noise and developed filtration algorithms to restore image quality (19). In the present work, we used an adaptive spatial median filter unless otherwise specified.

Signal and noise consideration with EMCCDs

Reading miniature PSDs in real time with a CCD camera is challenging because the light signal collected by the CCD camera is low. Previously, we used a larger PSD (1.4 mm^3 volume) and a longer acquisition time (5–20 s) (13,14). In this work we used an EMCCD to amplify the signal. EMCCDs are different from intensified CCDs (25). In intensified CCDs, incident photons are multiplied. In EMCCDs the charges stored in pixels are multiplied.

A CCD camera is affected by three sources of noise: 1) Quantum noise due to the discrete nature of photons; 2) Thermal noise; 3) Readout noise occurring when the pixels are digitized. Readout noise is relatively constant for a given readout frequency. In electron multiplying CCDs, the multiplication occurs before the pixels are read and this diminishes the relative importance of the readout noise. However this process does not affect the other two sources of noise. The multiplication process even adds noise (26). Consequently, electron multiplication is beneficial only when the readout noise dominates. More discussion on noise issues in amplified CCDs can be found elsewhere (25,26).

Electron multiplication is software-controlled and can be set to a value between 0 (no multiplication) and 255 (maximum multiplication). The relationship between this software setting and the actual gain in signal is not linear and was measured experimentally. A series of 100 identical, consecutive images were acquired in the reference conditions described above (i.e. 1.5 cGy per image) with electron multiplication settings of 0, 1 and 200. To avoid introducing bias from the noise filtration process, no filters were used to remove the impact of stray radiation on the CCD camera. Instead, a subset of 35 images that did not contain noise from stray radiation was selected from the original series for every gain level. For each PSD, pixel values were summed within a region of interest covering the whole light spot produced by that PSD (typically 150–200 pixels). The mean signal and standard deviation of this signal were then computed for the stack of 35 images. The average gain factor was found by comparing the amplified with the non-amplified readings.

Experimental setup

Real-time data acquisition was tested by irradiating 5 PSDs with the CCD camera in continuous acquisition mode at 150 ms per frame. Doses were delivered in segments of 200 cGy, 20 cGy, and 2 cGy. Readings were taken both as *near-instantaneous* dose measurements (*i.e.*, the dose delivered during a single CCD frame of 150 ms) and as *cumulative* dose measurements (*i.e.*, the total dose delivered in a particular segment). These measurements were made in an acrylic phantom at d_{max} (1.5 cm).

System performance was assessed by quantifying accuracy and precision. We delivered three 200-cGy irradiations to the phantom and analyzed the measured dose for each 150-ms frame. The first 10 frames of each series were excluded to eliminate variations that could result from the initial fluctuation of the linac's dose rate.

To test their ability to perform *in vivo* measurements, we mounted these PSDs onto two types of rectal balloons and inserted the PSD-equipped rectal balloon into an anthropomorphic prostate phantom (CIRS, Norfolk, VA). A CT scan was performed to acquire a reference CT image set. Then, the phantom was placed on the treatment couch and kilovoltage (kV) images were acquired with the on-board imaging (OBI) system to compare with the reference CT image and to determine the degree of visibility of these *in vivo* detectors. An 8-beam prostate IMRT treatment was then delivered to the phantom with the PSDs in place. The treatment plan was calculated using the Pinnacle^3 planning system (Philips Medical Systems, Cleveland, OH).

RESULTS

Signal-to-noise ratio (SNR)

PSD measurements are performed by summing all pixel values within a region of interest covering the light spot produced by the PSD. Under the above-mentioned reference conditions, the pixel values within a given light spot typically have mean values between 20 and 30 GSL, with a range of ~10 GSL to ~80 GSL. In these conditions, electron multiplication settings of 1 and 200 resulted in an average signal amplification gain factor of 2 and 40 respectively. Even with an electron multiplication setting of 200, we did not saturate the CCD and non-linearity was not observed. The SNR of the measured light spots was 35 for the image series without electron multiplication, 45 for the series with an electron multiplication setting of 1, and 70 for a setting of 40. As expected, the gain in SNR is smaller than the signal gain because of the increased noise seen in the amplified image. By studying the image on a pixel-by-pixel basis we found that electron multiplication improves the SNR for every pixel with a non-amplified value below 90 GSL and a deterioration of the SNR is seen for pixels above 1000 GSL.

Real-time data acquisition

The dose measured with the 5 PSDs every 150 ms over the delivery of 200 MU is shown in Fig. 3. All PSDs had a similar response and precision. All showed variations during the first second of irradiation due to the linac's initial adjustment of dose rate. Figure 4a–d shows the dose readings for total dose deliveries of 200 cGy for both a single PSD and the average of 5 PSDs. For both continuous dose delivery and equally weighted segments, the PSDs accurately measured both the near-instantaneous dose as well as the cumulative dose. All 5 PSDs produced similar dose measurements. We further tested the independence of the dose response per segment by delivering a series of 2-cGy segments (Table 1). For doses of 2 cGy, the PSD measurements were accurate within 2.3%.

Precision and accuracy

The histogram of the ratio of the measured dose to the delivered dose for three 200-cGy irradiations is shown in Fig. 5. A total of 1800 data points were included. The statistical distribution of the measurements was Gaussian, which is expected if the noise is solely of a stochastic nature.

The mean of the 5-PSD distribution was 0.9992, illustrating the high accuracy of the PSDs. The mean of the distribution of each individual PSD was also close to unity: 1.002, 1.000, 0.997, 1.002, and 0.994. The PSDs' precision, as measured from standard deviation of the distribution, was 3% for measurements performed every 150 ms (1.5 cGy), corresponding to an average of 50 linac pulses. Because image acquisitions were not synchronized to linac output, not every image contained the exact same number of pulses. A variation of one pulse would result a dose variation of ~2% between images, which is included in the measured standard deviation of 3%. The measurement standard deviation decreased rapidly for larger dose measurements (Table 1). Because the measurement distribution obeys Poisson statistics, the standard deviation of measurements comprising more than 1 frame will vary as the inverse of the square root of the total number of frames acquired for a given measurement. Figure 6 shows a plot of the estimated standard deviation as a function of the total measured dose assuming that images were acquired every 150 ms and of the measured standard deviation for the measurements listed in Table 1. There is a good fit between the estimated and measured standard deviations.

Feasibility of in vivo applications

The PSDs were compatible with two clinical models of rectal balloons (Fig. 1e) and easily inserted into the anthropomorphic phantom. Because of their miniature size, the PSDs were difficult to detect; they could be seen in the CT image (Fig. 7a), but not in the kV images (Figs. 7b–7c). However, in the kV images, their position can be inferred from the location of clearly visible markers such as the stem of the balloon, the surface of the balloon, or a radio-opaque marker placed 7-cm proximal to the dose-sensitive region of the PSDs. Results for the 8-beam IMRT treatment delivered to the phantom are shown in Fig. 8. The dose for each individual PSD and the median dose of all 5 PSDs are compared for each beam to the median dose obtained from the treatment planning system. Even in such a high dose gradient, good agreement is seen between the planned and measured doses. Overall, for all beams, the PSDs agreed with the treatment plan to within 0.5%

DISCUSSION

Complex dynamic treatments such as dynamic IMRT, tomotherapy, and volumetric modulated arc therapy produce strong dose gradients in space and time. Even with the use of 4D imaging and 4D treatment planning systems, dose distributions may be affected by sudden patient movements. Real-time *in vivo* dosimeters can monitor dose delivery and detect deviations from the original treatment plan. At the present time, only a handful of dosimeters can be used *in vivo*. The most commonly used dosimeters are TLDs, which do not provide real-time measurements, and diodes (2). Other detectors, such as MOSFETs (9) and OSL detectors (5,21), have also been used for real-time *in vivo* measurements. In this work, we have shown that a PSD system can serve as a real-time *in vivo* dosimetry system.

Our results show that *in vivo dose* monitoring with PSDs is feasible and will be tested on a small number of patients in the near future. Further development is required before they are ready for daily clinical use. For ease of use and transportation, the compact reading apparatus needs to be placed inside a more convenient support and housing that includes a reproducible connector mechanism similar to that used with the offline dosimeter array (14).

With such a support, detector calibration would be required after 9 hours of exposure at a dose rate of 600 MU/min. At 5 patients per day each receiving about 2Gy, the detector will need to be calibrated once a year. In addition, software should be developed to facilitate image acquisition and processing, detector calibration and data storage.

With the PSD system described here, the measurement uncertainty was 3% (1 standard deviation) for an acquisition time of 150 ms, equivalent to a dose of 1.5cGy. The precision improved with increasing dose; at 200 cGy, the standard deviation was 0.4%. In contrast, the precision of diodes has been reported to be greater than 1% for doses between 32 to 385 cGy (22). Moreover, for TLDs irradiated to doses of ~300 cGy, the standard deviation has been reported as 1.5% for individual readings (23).

A real-time *in vivo* detector system offers all the advantages of an integrating, offline detector plus the capability to determine the exact moment when deviations between the planned and delivered doses occurred. We plan to use this information in our adaptive radiation therapy treatment procedure. The first use of the real-time dose information is as a warning mechanism. By monitoring dose continuously, we can detect any sudden deviation from the expected dose and if it exceeds a certain threshold we can stop the treatment, re-position the patient and resume. The second use of the PSD system is to evaluate if a change in the dose prescription or a re-planning is required between fractions. This is similar to what could be achieved with an integrating offline detector, but with the added knowledge of when discrepancies occur. This information can be used to determine if a single field should be adjusted or, if the patient motion is too large in a given direction, the margins should be changed.

Shorter acquisition times could be used, but at the cost of higher uncertainty per frame. In contrast, longer acquisition times or better light collection efficiency (24) could further reduce the uncertainty per frame. Larger PSDs could also be used to reduce the uncertainty per frame, but at the expense of spatial resolution. Smaller PSDs are especially important if they are to be used in conjunction with medical devices to provide *in vivo* measurements; however, larger PSDs could be used to measure entry and/or exit doses.

CONCLUSION

PSDs are highly versatile dose detectors. Their water equivalence, dose linearity, and energy independence make them useful in modern radiation therapy, where the use of complex dose distributions is rapidly becoming standard clinical practice.

Our main findings are as follows: (a) a PSD multi-probe array can be read in real time with a CCD-based acquisition apparatus; (b) PSDs with a high spatial resolution (0.4 mm^3) can be mounted on a clinical rectal balloon and used for *in vivo* dose measurements; (c) the precision of the PSDs was 3% for measurements performed every 150 ms (1.5 cGy) and improved to 0.4% for a total dose of 200 cGy; (d) the accuracy of the PSDs was high, with a ratio between the measured to expected dose of 0.9992. We conclude that this PSD system can be used to directly measure the dose delivered to organs at risk, critical structures, and near the target during prostate irradiation. In the future, we will use these PSDs in conjunction with other medical devices such as urinary catheters and rectal balloons to perform *in vivo* dose measurements in real time in patients treated with dynamic radiation treatment modalities such as dynamic IMRT, tomotherapy, and volumetric modulated arc therapy.

Acknowledgments

This research was supported in part by the National Cancer Institute (1R01CA120198-01A2). One author (L.A.) was supported in part by the Odyssey program and the Houston Endowment, Inc., Award for Scientific Achievement at The University of Texas M. D. Anderson Cancer Center.

REFERENCES

1. deCrevoisier R, Tucker S, Dong L, et al. Increased risk of biochemical and local failure in patients with distended rectum on the planning CT for prostate cancer radiotherapy. International journal of radiation oncology, biology, physics 2005;62:965–973.
2. Essers M, Mijnheer B. *In vivo* dosimetry during external photon beam radiotherapy. International journal of radiation oncology, biology, physics 1999;43:245.
3. Rink A, Vitkin I, Jaffray D. Characterization and real-time optical measurements of the ionizing radiation dose response for a new radiochromic medium. Medical Physics 2005;32:2510–2516. [PubMed: 16193781]
4. Rink A, Vitkin I, Jaffray D. Suitability of radiochromic medium for real-time optical measurements of ionizing radiation dose. Medical Physics 2005;32:1140–1155. [PubMed: 15895598]
5. Andersen C, Marckmann C, Aznar M, et al. An algorithm for real-time dosimetry in intensity-modulated radiation therapy using the radioluminescence signal from Al2O3:C. Radiation protection dosimetry 2006;120:7–13. [PubMed: 16644973]
6. Briere T, Tailor R, Tolani N, et al. Patient dosimetry for total body irradiation using single-use MOSFET detectors. Journal of applied clinical medical physics 2008;9:2787. [PubMed: 19020482]
7. Ciocca M, Piazzi V, Lazzari R, et al. Real-time *in vivo* dosimetry using micro-MOSFET detectors during intraoperative electron beam radiation therapy in early-stage breast cancer. Radiotherapy and oncology 2006;78:213–216. [PubMed: 16359743]
8. Cherpak A, Ding W, Hallil A, Cygler J. Evaluation of a novel 4D *in vivo* dosimetry system. Medical Physics 2009;36:1672–1679. [PubMed: 19544784]
9. Lambert J, Nakano T, Law S, et al. *In vivo* dosimeters for HDR brachytherapy: a comparison of a diamond detector, MOSFET, TLD, and scintillation detector. Medical Physics 2007;34:1759. [PubMed: 17555257]
10. Beddar A. Water equivalent plastic scintillation detectors in radiation therapy. Radiation protection dosimetry 2006;120:1–6. [PubMed: 16882685]
11. Beddar A, Mackie T, Attix F. Water-equivalent plastic scintillation detectors for high-energy beam dosimetry: I. Physical characteristics and theoretical consideration. Physics in Medicine and Biology 1992;37:1883–1900. [PubMed: 1438554]
12. Beddar A, Mackie T, Attix F. Water-equivalent plastic scintillation detectors for high-energy beam dosimetry: II. Properties and measurements. Physics in Medicine and Biology 1992;37:1901–1913. [PubMed: 1438555]
13. Archambault L, Beddar A, Gingras L, et al. Water-equivalent dosimeter array for small-field external beam radiotherapy. Medical Physics 2007;34:1583. [PubMed: 17555240]
14. Lacroix F, Archambault L, Gingras L, et al. Clinical prototype of a plastic water-equivalent scintillating fiber dosimeter array for QA applications. Medical Physics 2008;35:3682. [PubMed: 18777928]
15. Archambault L, Arsenault J, Gingras L, et al. Plastic scintillation dosimetry: Optimal selection of scintillating fibers and scintillators. Medical Physics 2005;32:2271. [PubMed: 16121582]
16. Archambault L, Beddar A, Gingras L, et al. Measurement accuracy and cerenkov removal for high performance, high spatial resolution scintillation dosimetry. Medical Physics 2006;33:128–135. [PubMed: 16485419]
17. Fontbonne J, Iltis G, Ban G, et al. Scintillating fiber dosimeter for radiation therapy accelerator. IEEE Transactions on Nuclear Science 2002;49:2223–2227.
18. Frelin A, Fontbonne J, Ban G, et al. Spectral discrimination of Cerenkov radiation in scintillating dosimeters. Medical Physics 2005;32:3000. [PubMed: 16266114]

19. Archambault L, Briere TM, Beddar S. Transient noise characterization and filtration in CCD cameras exposed to stray radiation from a medical linear accelerator. Medical Physics 2008;35:4342–4351. [PubMed: 18975680]

20. Vargas C, Saito A, Hsi W, et al. Cine-Magnetic Resonance Imaging Assessment of Intrafraction Motion for Prostate Cancer Patients Supine or Prone With and Without a Rectal Balloon. American journal of clinical oncology. 2009 in press.

21. Jursinic P. Characterization of optically stimulated luminescent dosimeters, OSLDs, for clinical dosimetric measurements. Medical Physics 2007;34:4594–4604. [PubMed: 18196786]

22. Rodriguez M, Abrego E, Pineda A. Implementation of *in vivo* Dosimetry with Isorad Semiconductor Diodes in Radiotherapy. Medical Dosimetry 2008;33:14–21. [PubMed: 18262118]

23. Kirby T, Hanson W, Johnston D. Uncertainty analysis of absorbed dose calculations from thermoluminescence dosimeters. Medical Physics 1992;19:1427–1433. [PubMed: 1461205]

24. Beddar A, Law S, Suchowerska N, Mackie T. Plastic scintillation dosimetry: optimization of light collection efficiency. Physics in Medicine and Biology 2003;48:1141–1152. [PubMed: 12765328]

25. Perera H, Williamson J, Monthofer S, et al. Rapid two-dimensional dose measurement in brachytherapy using plastic scintillator sheet: linearity, signal-to-noise ratio, and energy response characteristics. International journal of radiation oncology, biology, physics 1992;23:1059–1069.

26. Robbins MS, Hadwen BJ. The Noise Performance of Electron Multiplying Charge-Coupled Devices. ieee trans. Nucl. sci 2000;50:1227–1232.

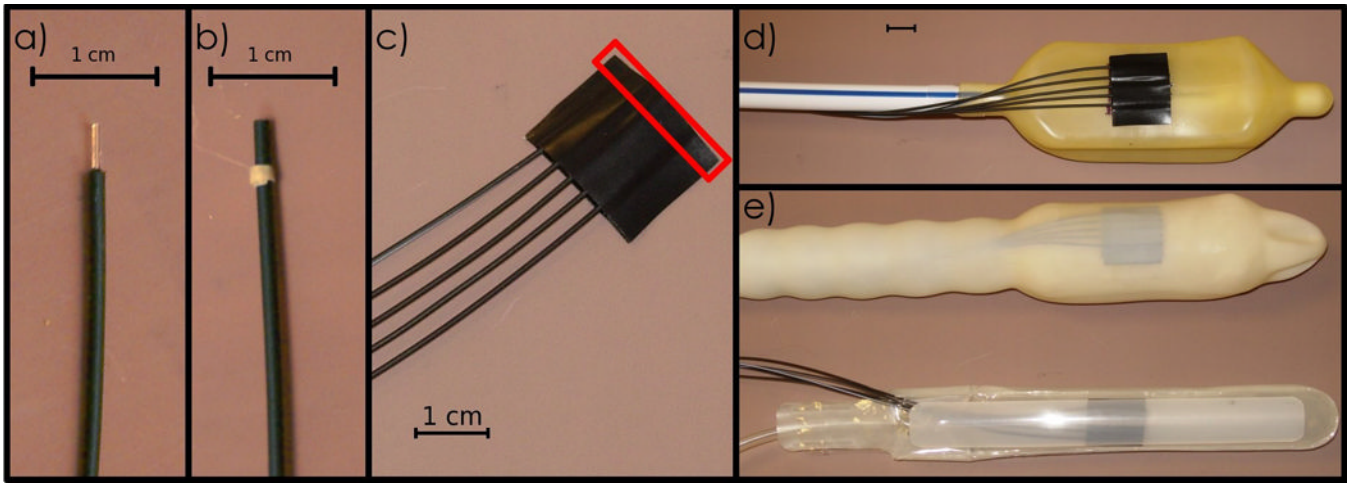

Fig. 1.

a) A single PSD with its scintillator component bare. b) A PSD completely protected by a black polyethylene jacket to shield it from ambient light. c) A detector patch of 5 PSDs. The red rectangle illustrates the dose-sensitive region. d) A detector patch mounted onto a rectal balloon. e) Two models of rectal balloons equipped with PSDs ready for use as *in vivo* dosimeters.

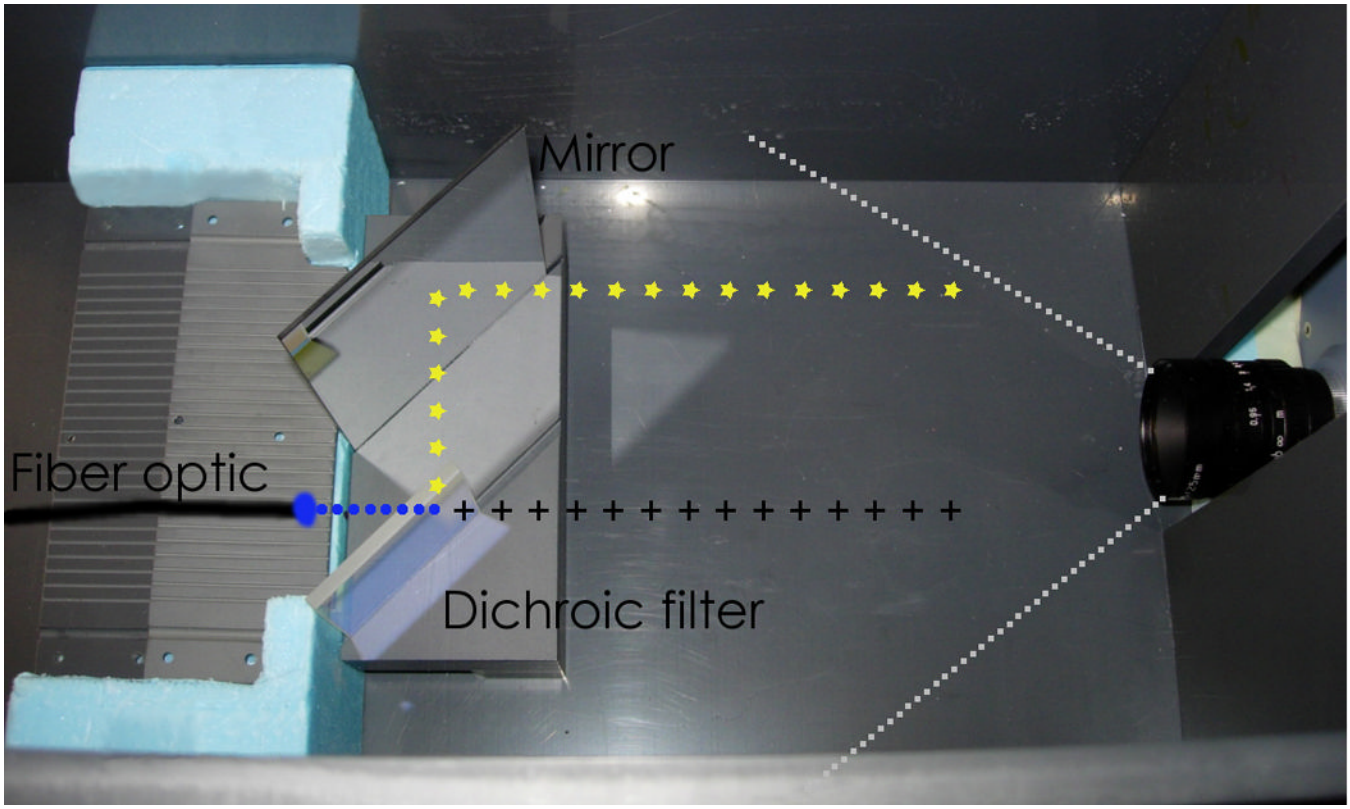

Fig. 2.
The apparatus used for reading the PSDs. An illustration of light propagation is overlaid. The light emitted from the optical fiber (circles) travels to the 45°-dichroic filter, where it is divided into a transmitted component (crosses) and a reflected component (stars).

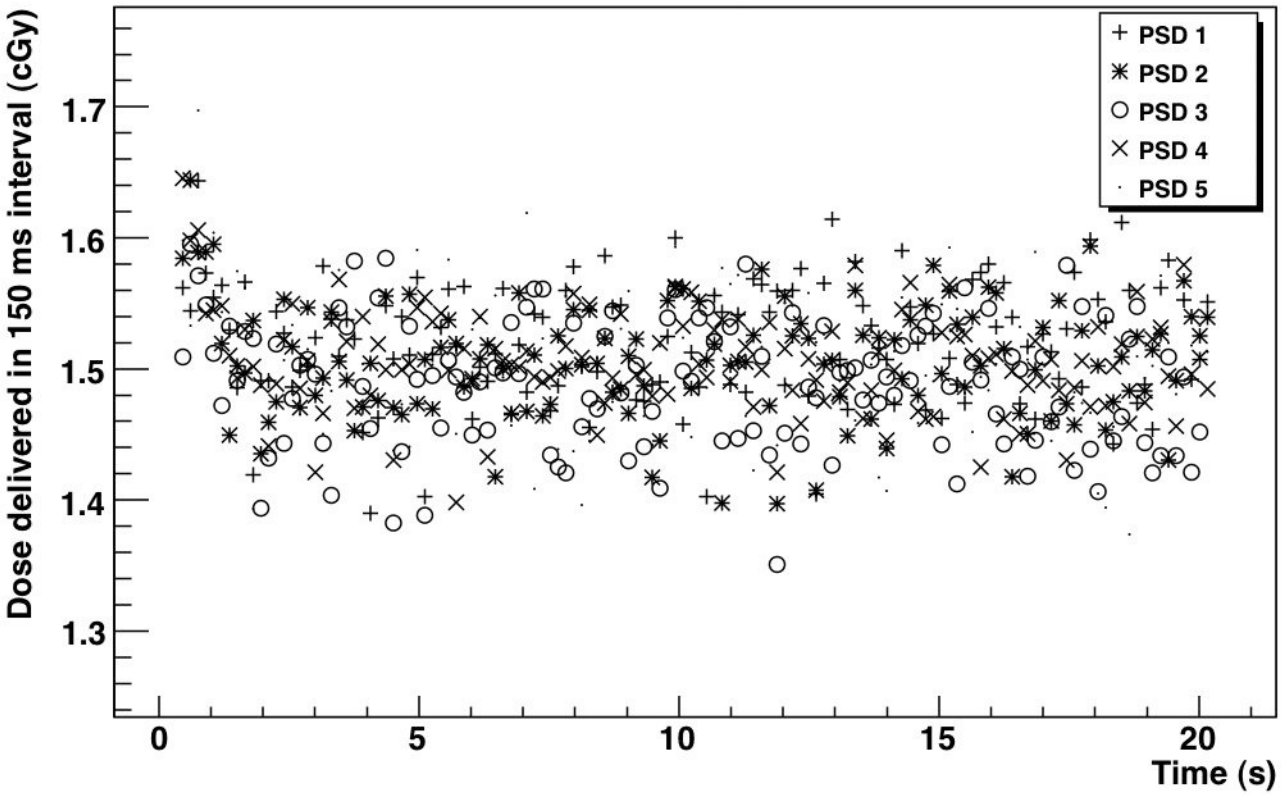

Fig. 3.
Dose measured with the 5 PSDs every 150 ms over the delivery of 200 MU.

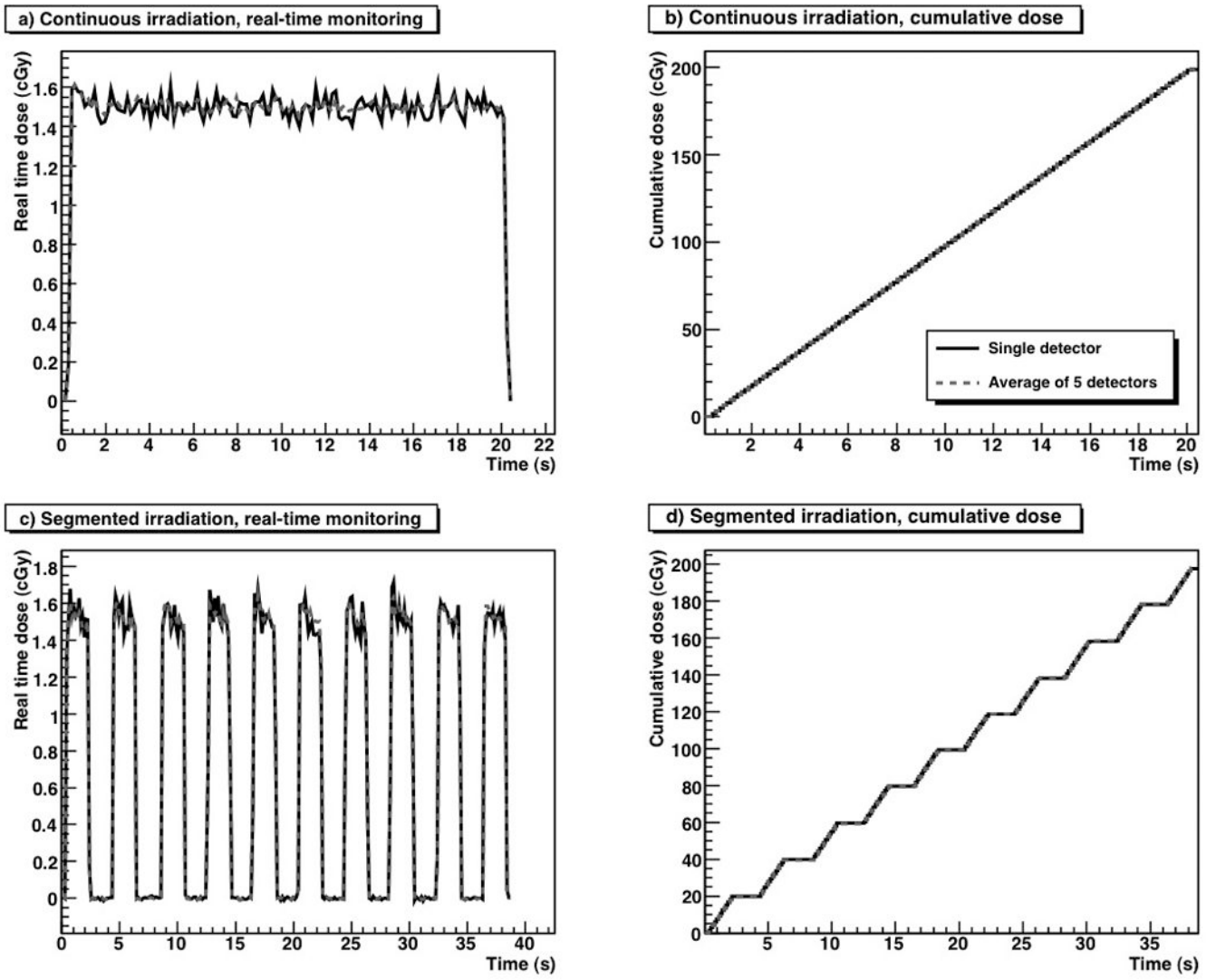

Fig. 4.

a) Real-time monitoring, and b) a cumulative dose of 200 cGy delivered continuously. c) Real-time monitoring and d) a cumulative dose of 200 cGy delivered in 10 equally weighted 20-cGy segments.

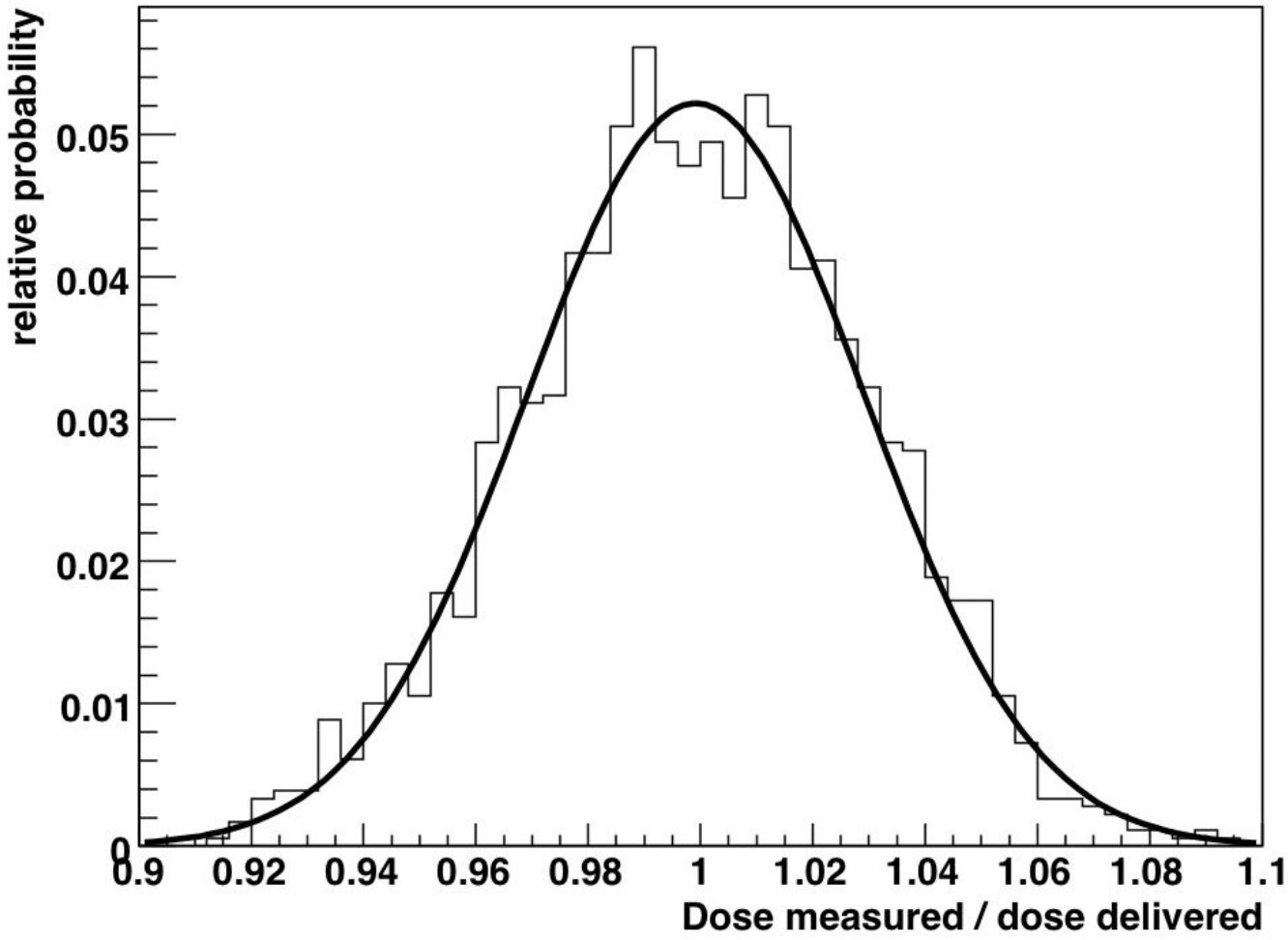

Fig. 5.
Statistical distribution of the measured dose compared to the delivered dose read at 150 ms. The black line represents a Gaussian fit to the data.

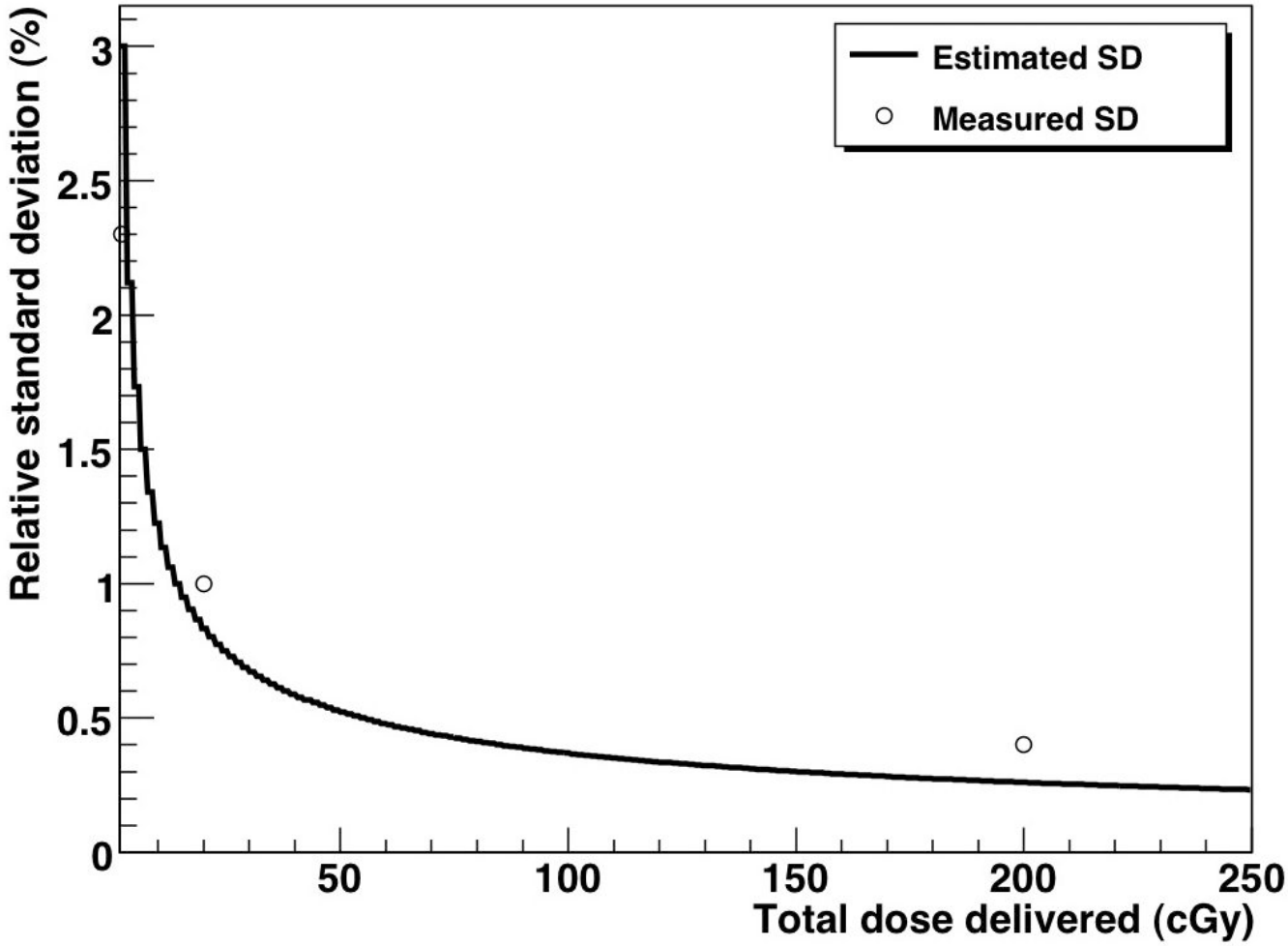

Fig. 6.
Measured and estimated standard deviation of the PSD system as a function of total delivered dose.

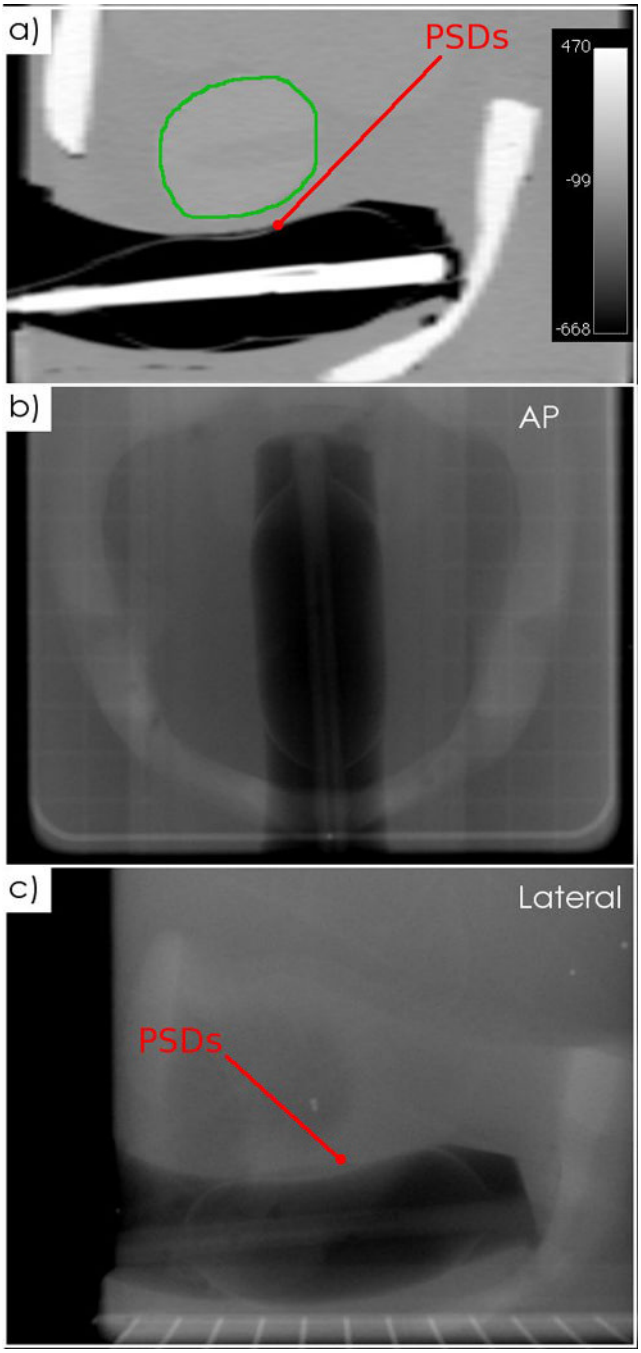

Fig. 7.
CT and kV images of the PSDs inserted into an anthropomorphic phantom. a) A sagittal CT slice with the prostate contoured (green), showing the PSDs. b) An anteroposterior kV image and c) a lateral kV image acquired with the linac's OBI system.

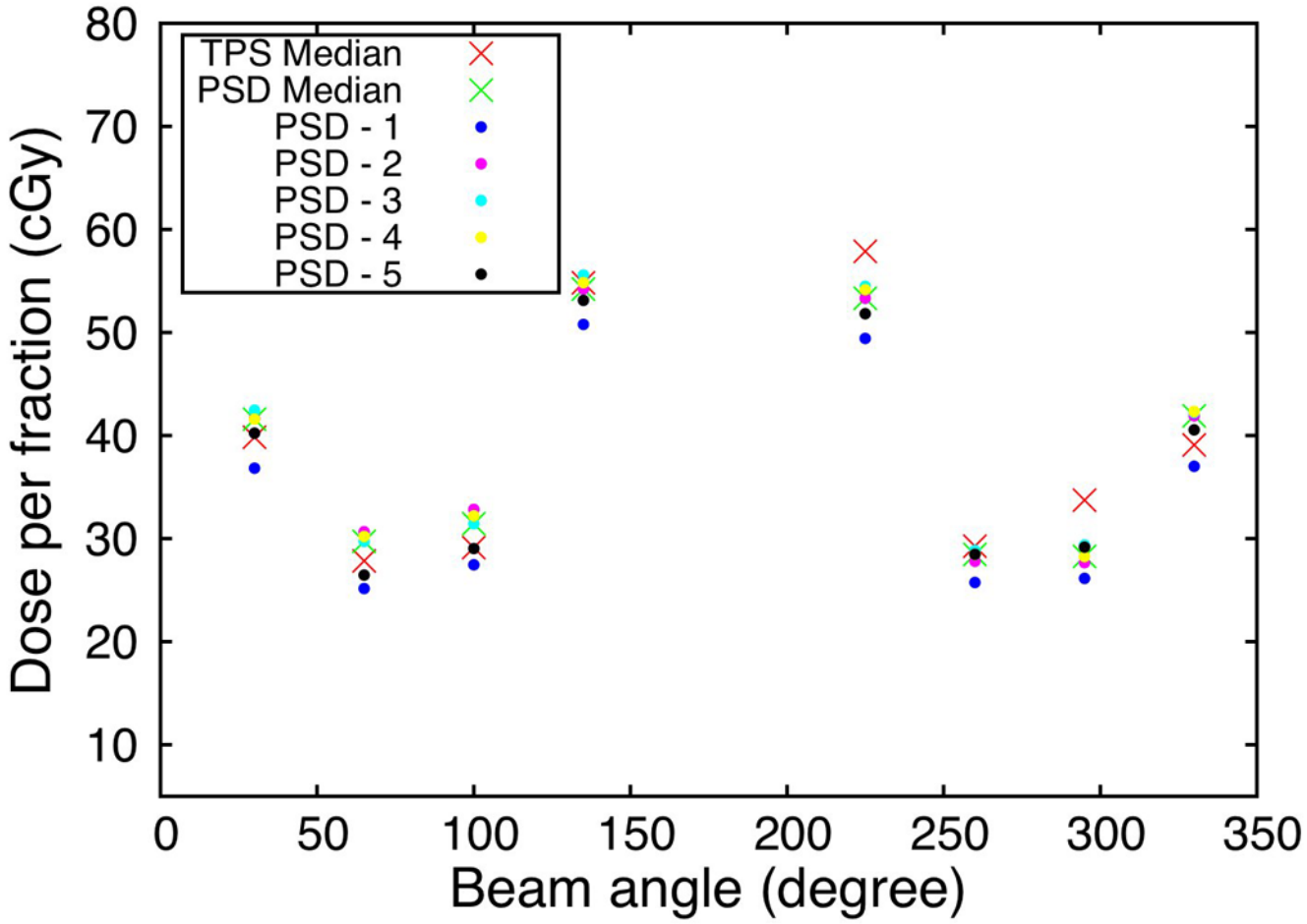

Fig. 8.
Dose measured in the anthropomorphic phantom for the 5 PSDs mounted on the rectal probe compared to the dose predicted by the treatment planning system.

Table 1

Measured reproducibility of delivered doses between 2 and 200 cGy

Delivered dose (cGy)	Measured dose / Delivered dose	Standard deviation (%)
200	0.997	0.4
20	0.996	1.0
2	1.021	2.3